RESEARCH   **Open Access**

A decomposition formula for the wall heat flux of a compressible boundary layer

Dong Sun[1], Qilong Guo[1], Xianxu Yuan[1,2], Haoyuan Zhang[1,2], Chen Li[1*] and Pengxin Liu[1*]

* Correspondence: lichen@skla.
cardc.cn; liupengxin@cardc.cn
[1]State Key Laboratory of
Aerodynamics, Mianyang 621000,
Sichuan, China
Full list of author information is
available at the end of the article

Abstract

Understanding the generation mechanism of the heat flux is essential for the design of hypersonic vehicles. We proposed a novel formula to decompose the heat flux coefficient into the contributions of different terms by integrating the conservative equation of the total energy. The reliability of the formula is well demonstrated by the direct numerical simulation results of a hypersonic transitional boundary layer. Through this formula, the exact process of the energy transport in the boundary layer can be explained and the dominant contributors to the heat flux can be explored, which are beneficial for the prediction of the heat and design of the thermal protection devices.

Keywords: Heat flux, Hypersonic boundary layer, Direct numerical simulation

1 Introduction

The heat transfer prediction is of great importance for hypersonic vehicles. When the transition or turbulence happens, the accurate prediction becomes even more challenging. Therefore, exploring the generation mechanism of the heat flux has drawn wide attention. Many efforts have been put into understanding the generation mechanism of the heat flux, which provides important guidance for the design of the thermal protection system and the thermal management [1].

Some efforts took advantage of the similarities between the generation of friction and heat flux, and constructed the Reynolds analogy [2] $Ra = 2St/C_f$ to connect friction with heat flux, where St is the Stanton number, C_f the skin friction coefficient. Hopkins and Inouye [3] predicted the surface heat flux of the hypersonic boundary layer with $Ra = 1$. However, the accuracy of this correlation decreases significantly on a cold wall at high Mach numbers. More intrinsic mechanisms should be considered. Huang et al. [4] derived the formula $q_w = -u_b \tau_w$ by the assumption that the heat transfer into the walls equals the total pressure work done across the channel. Chen et al. [5] established the exact relations for the skin friction with other dynamic and kinetic quantities, and they found these relations revealed that the skin friction is intrinsically coupled with the surface temperature through the heat flux. Abe and Antonia [6] proposed a simple relation between the scalar dissipation rate and the wall heat transfer coefficient for the channel flow. Kim et al. [7] proposed a direct approach for the time-

dependent heat flux by assuming the temperature approximated as a third-order polynomial of position. Ebadi et al. [8] obtained the wall heat flux by a triple integration of the Reynolds averaged energy equation for the two-dimensional incompressible turbulent boundary layer. Fukagata et al. [9] studied the relationship of the wall heat flux and the Nusselt number in the incompressible channel. And the similar relation was obtained by Liu [10] when studying the compressible pipe flow. Ghosh [11] proposed that the wall heat flux can be expressed by the sum of the integrations of different viscous terms in the incompressible turbulent channel and pipe flow. Zhang and Xia [12] further proposed a formula to assess the contributions of the viscous stresses to the heat transfer in a turbulent channel flow by the method of Fukagata et al. [13], but the turbulent stresses were missing in their expression due to the simplification assumptions used in the channel flow.

Previous studies have not built the relation of the generation mechanism of the heat flux to the dynamic energy transport of the compressible boundary layer. Therefore, a more reliable and accurate method to gain insights into the generation mechanism should be derived. In the paper, we propose a new decomposition formula for the wall heat flux by integrating the conservation equation of total energy, which can explain the energy transport process in the boundary layer and reveal the main factors affecting the wall heat flux. As far as the authors' knowledge, this is the first decomposition formula proposed for the wall heat flux of the compressible boundary layer. The new formula is derived by the method of Renard et al. [14], which is more physical and feasible than those [11, 12] based on the method of Fukagata et al. [13] It serves an insight into the complex transport processes of the wall heat flux, and helps us find the key factors.

The work of this paper is organized as follows. In section 2, we describe numerical methods and case setup in brief. In section 3, the detailed derivation of the decomposition formula is presented. In section 4, the validation of the DNS of a hypersonic transitional boundary layer is performed, and the proposed decomposition formula is applied to analyze the heat flux. Finally, some conclusions are drawn in section 5.

2 Numerical methods and case setup

To analyze the heat flux decomposition of the hypersonic transitional boundary layer, a direct numerical simulation is performed. The compressible Navier-Stokes equations in the curvilinear coordinate are adopted as governing equations.

$$\frac{\partial \rho}{\partial t} + \frac{\partial \rho u_j}{\partial x_j} = 0 \tag{1a}$$

$$\frac{\partial \rho u_i}{\partial t} + \frac{\partial \rho u_i u_j}{\partial x_j} + \frac{\partial p \delta_{ij}}{\partial x_j} = \frac{\partial \sigma_{ij}}{\partial x_j} \tag{1b}$$

$$\frac{\partial \rho e}{\partial t} + \frac{\partial u_j(\rho e + p)}{\partial x_j} = \frac{\partial u_j \sigma_{ij}}{\partial x_j} + \frac{\partial q_j}{\partial x_j} \tag{1c}$$

Where u_1, u_2 *and* u_3 are streamwise, normal and spanwise velocities, respectively. And p and ρ are pressure and density. The expressions of ρe, σ_{ij}, and q_j are defined as

$$\rho e = \frac{p}{\gamma - 1} + \frac{1}{2}\rho\left(u^2 + v^2 + w^2\right) \tag{2}$$

$$\sigma_{ij} = \frac{\mu}{Re_\infty}[(\frac{\partial u_i}{\partial x_j} + \frac{\partial u_j}{\partial x_i}) - \frac{2}{3}\delta_{ij}\frac{\partial u_k}{\partial x_k}] \tag{3}$$

$$q_j = \frac{\mu}{PrMa_\infty^2 Re_\infty(\gamma-1)}\frac{\partial T}{\partial x_j}. \tag{4}$$

The usual indicial notation is used. Prandtl number Pr is set as 0.72 and the specific heat ratio γ is 1.4. The dynamic viscosity μ is obtained by using Sutherland's law. Ma_∞ is the freestream Mach number and Re_∞ is the Reynolds number. The working fluid is air, and the gas model is assumed to be the perfect gas model.

An in-house code with high-order schemes is employed to perform the DNS. This code has been applied in many DNS simulations of compressible turbulent cases, including compressible homogeneous turbulence [15], turbulent boundary layer [15] and shock wave/boundary layer interaction [16–18]. The accuracy and robustness have been well validated. The hybrid optimized WENO scheme is adopted to discretize the inviscid fluxes with a novel discontinuity detector [19]. In the regions with discontinuities, a seventh-order WENO scheme [20] is activated and in the smooth region, a fourth-order bandwidth-optimized upwind-biased scheme [19] is used to resolve the small structures in the turbulent boundary layer. The viscous terms are discretized by the fourth-order central scheme. The third-order TVD Runge-Kutta method is adopted as the temporal algorithm. Ma_∞ is set as 6.0, and Re_∞ is 12,000 which is based on the millimetre and freestream parameters. The freestream temperature is 65 K and the wall temperature is 305 K. The millimetre is adopted as the reference length.

The sketch of the computational domain is presented in Fig. 1. The lengths in the streamwise, normal and spanwise direction are $L_x = 416$, $L_y = 35$ and $L_z = 14$, respectively. The computational domain is discretized with $N_x \times N_y \times N_z = 1151 \times 320 \times 149$ points. The grid points are equally spaced in the spanwise direction, and clustered near the wall in the normal direction. The grid spacing normalized by the wall unit in the three directions is $dx^+ = 7.9$, $dy_w^+ = 0.36$ and $dz^+ = 3.4$, respectively. A hypersonic laminar profile is fixed at the inlet. The outlet boundary condition is a supersonic outflow with a sponge layer to further suppress the disturbances originated from the outlet. The upper boundary is a non-reflective condition. And an isothermal nonslip condition is applied at the wall. The periodical conditions are set on both sides in the spanwise direction. To trigger a bypass transition, a blow and suction forcing method is employed, which sets a normal
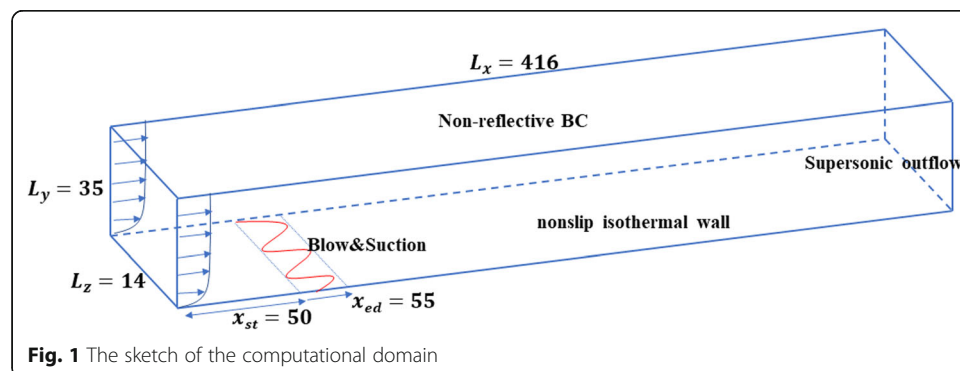

Fig. 1 The sketch of the computational domain

velocity disturbance $v_n = Af(x)\, cos\,(2\pi\lambda_z/L_z)$ at the wall, where $f(x)$ is used to control the streamwise extent of force [21], λ_z is the spanwise wavelength and is set as 4.0 in the present simulation. The forcing region ranges from $x = 50$ to $x = 55$.

3 Derivation of the decomposition formula

Under the assumption of homogeneity in the spanwise direction and nonslip condition at the wall, the time-averaged conservative equations for the specific total energy can be expressed as,

$$\bar{\rho}\frac{D\tilde{E}}{Dt} + \frac{\partial \bar{p}\tilde{u}_j}{\partial x_j} = \frac{\partial}{\partial x_j}\left(q_{L,j} + q_{T,j} + D_j + T_j + MS_j + RS_j\right) \tag{5}$$

when ϕ is an arbitrary variable, $\bar{\phi}$ denotes Reynolds average, $\tilde{\phi}$ Favre average and $\phi^{''}$ is the fluctuations concerning the Favre average. $\tilde{E}$ denotes the specific total energy, $q_{L,j}$ the heat conduction, $q_{T,j}$ the turbulent transport of heat, D_j the molecular diffusion, T_j the turbulent transport of turbulent kinetic energy (TKE), MS_j work by the molecular stresses and RS_j work by Reynold stresses. In Table 1, the specific expressions of the terms at the right hand of Eq. (5) are presented. More details about Eq. (5) can be found in the book of Wilcox [22].

The work of Renard [14] and Li [23] about skin friction decomposition provides good hints for building the integration relation of heat flux. In order to isolate the effects of the energy transport terms, the absolute reference frame is employed. The reference absolute frame is attained by assuming that the wall moves at the speed U_∞. The expressions of the time t_a, coordinates x_a, y_a, velocities u_a, v_a, pressure p_a and the density ρ_a in the reference absolute frame satisfy

$$\begin{aligned} t_a &= t, \quad x_a = x - U_\infty t, \quad y_a = y, \\ u_a &= u - U_\infty, \quad v_a = v, \\ p_a &= p, \quad \rho_a = \rho \end{aligned} \tag{6}$$

where the subscript 'a' represents 'absolute' variables under the reference frame. By substituting Eq. (6) into Eq. (5), Eq. (5) takes the form

Table 1 Expressions for the terms at the right hand of Eq. (5)

Heat conduction	$q_{L,j} = \overline{\kappa \partial T/\partial x_j}$
Turbulent transport of heat	$q_{T,j} = -\overline{\rho u_j'' h''}$
Molecular diffusion	$D_j = \overline{u_k'' \sigma_{kj}}$
Turbulent transport of TKE	$T_j = \overline{\rho u_j'' u_k'' u_k''}/2$
Work by molecular stresses	$MS_j = \tilde{u}_k \bar{\sigma}_{k,j}$
Work by Reynolds stresses	$RS_j = -\tilde{u}_k \overline{\rho u_k'' u_j''}$

$$\bar{\rho}_a \frac{D\tilde{E}_a}{Dt_a} + \frac{\partial(\bar{p}_a\tilde{u}_a)}{\partial(x_a + U_\infty t_a)} + \frac{\partial(\bar{p}_a\tilde{v}_a)}{\partial y_a}$$

$$= \frac{\partial}{\partial y_a}(q_{L,y,a} + q_{T,y,a} + D_{y,a} + T_{y,a} + MS_{y,a} + RS_{y,a}) \tag{7}$$

$$+ \frac{\partial}{\partial(x_a + U_\infty t_a)}(q_{L,x,a} + q_{T,x,a} + D_{x,a} + T_{x,a} + MS_{x,a} + RS_{x,a})$$

By multiplying $\tilde{u}_a$ at both sides of Eq. (7), combining the continuity equation and moving the heat fluxes in the normal direction to the left side and all the other terms to the right, the following equation could be obtained,

$$\tilde{u}_a \frac{\partial}{\partial y_a}(q_{L,y,a} + q_{T,y,a})$$

$$= \tilde{u}_a\bar{\rho}_a \frac{D\tilde{E}_a}{Dt_a} + \tilde{u}_a \frac{\partial(\bar{p}_a\tilde{u}_a)}{\partial(x_a + U_\infty t_a)} + \tilde{u}_a \frac{\partial(\bar{p}_a\tilde{v}_a)}{\partial y_a}$$

$$- \tilde{u}_a \frac{\partial}{\partial y_a}(D_{y,a} + T_{y,a} + MS_{y,a} + RS_{y,a}) \tag{8}$$

$$- \tilde{u}_a \frac{\partial}{\partial(x_a + U_\infty t_a)}(q_{L,x,a} + q_{T,x,a} + D_{x,a} + T_{x,a} + MS_{x,a} + RS_{x,a})$$

Integrating Eq. (8) from the wall to the farfield, the heat flux on the wall ($y = 0$) can be expressed as the following form.

$$q_{L,y,a}|_{y=0} =$$

$$\frac{1}{U_\infty} \int_0^\infty [(q_{L,y,a} + q_{T,y,a}) \frac{\partial \tilde{u}_a}{\partial y_a}] dy$$

$$- \frac{1}{U_\infty} \int_0^\infty [\tilde{u}_a \frac{\partial}{\partial y_a}(D_{y,a} + T_{y,a} + MS_{y,a} + RS_{y,a})] dy \tag{9}$$

$$+ \frac{1}{U_\infty} \int_0^\infty [\tilde{u}_a\bar{\rho}_a \frac{D\tilde{E}_a}{Dt_a} + \tilde{u}_a \frac{\partial(\bar{p}_a\tilde{u}_a)}{\partial(x_a + U_\infty t_a)} + \tilde{u}_a \frac{\partial(\bar{p}_a\tilde{v}_a)}{\partial y_a}] dy$$

$$- \frac{1}{U_\infty} \int_0^\infty [\tilde{u}_a \frac{\partial}{\partial(x_a + U_\infty t_a)}(q_{L,x,a} + q_{T,x,a} + D_{x,a} + T_{x,a} + MS_{x,a} + RS_{x,a})] dy$$

Finally, Eq. (9) can be transformed into the initial frame and the heat flux coefficient is obtained by introducing the definition of the coefficient $C_h = \frac{1}{\rho_\infty U_\infty^3} \kappa \frac{\partial T}{\partial y}\big|_{y=0}$,

$$C_{h,decomp} = \underbrace{\frac{1}{\rho_\infty U_\infty^4} \int_0^\infty q_{L,y} \frac{\partial \tilde{u}}{\partial y} dy}_{C_{h,1}} + \underbrace{\frac{1}{\rho_\infty U_\infty^4} \int_0^\infty q_{T,y} \frac{\partial \tilde{u}}{\partial y} dy}_{C_{h,2}} - \underbrace{\frac{1}{\rho_\infty U_\infty^4} \int_0^\infty (\tilde{u} - U_\infty) \frac{\partial D_y}{\partial y} dy}_{C_{h,3}}$$

$$- \underbrace{\frac{1}{\rho_\infty U_\infty^4} \int_0^\infty (\tilde{u} - U_\infty) \frac{\partial T_y}{\partial y} dy}_{C_{h,4}} - \underbrace{\frac{1}{\rho_\infty U_\infty^4} \int_0^\infty (\tilde{u} - U_\infty) \frac{\partial MS_y}{\partial y} dy}_{C_{h,5}} - \underbrace{\frac{1}{\rho_\infty U_\infty^4} \int_0^\infty (\tilde{u} - U_\infty) \frac{\partial RS_y}{\partial y} dy}_{C_{h,6}}$$

$$+ \underbrace{\frac{1}{\rho_\infty U_\infty^4} \int_0^\infty (\tilde{u} - U_\infty)[\bar{\rho}\frac{D\tilde{E}}{Dt} + \frac{\partial \bar{p}\tilde{u}}{\partial x} + \frac{\partial \bar{p}\tilde{v}}{\partial y} - \frac{\partial}{\partial x}(q_{L,x} + q_{T,x} + D_x + T_x + MS_x + RS_x)] dy}_{C_{h,7}}$$

$$\tag{10}$$

In Eq. (10), the heat flux coefficient $C_{h,decomp}$ has been decomposed into seven parts, i.e., $C_{h,1}$ to $C_{h,7}$. The first part $C_{h,1}$ represents the contribution of heat conduction, the

second part $C_{h,2}$ the turbulent transport of heat, the third part $C_{h,3}$ the normal component of the molecular diffusion, the fourth part $C_{h,4}$ the turbulent transport of turbulent kinetic energy (TKE), the fifth part $C_{h,5}$ the work by the molecular stresses and the sixth part $C_{h,6}$ the work by Reynolds stresses. And the last part $C_{h,7}$ contains the streamwise heterogeneity, pressure work and the variation of the specific total energy with time.

4 Decomposition results of the wall heat flux

In this section, the reliability and accuracy of the new decomposition formula will be demonstrated by the DNS results of a hypersonic transitional boundary layer. The contributions of different energy transport processes such as the heat conduction, the turbulent transport of heat, the work done by molecular stresses will be calculated. Moreover, the key normal locations where the structures impact the wall heat will be assessed by the integrand functions of these contributions.

4.1 DNS results of the hypersonic transitional boundary layer

The instantaneous vortical structures displayed by Q criterion [24] are presented in Fig. 2. The transition process can be observed. Three streamwise locations (P1, P2 and P3) are chosen to validate the decomposition results, which are marked by shade planes. In Fig. 3, the mean streamwise velocity after van Driest transformation at P3 is presented and compared with DNS results of hypersonic results by Priebe [25]. Good agreement is obtained. The discrepancy in the outer part of the boundary layer is caused by the different friction velocity at the wall. In Fig. 4, the Reynolds stresses normalized by the friction velocity are presented. Several supersonic and hypersonic results [26–28] are also displayed. The information of the setup of reference simulations is presented in Table 2, where δ_{ref} is the nominal boundary layer thickness in the fully developed region. The present data generally agree with those in the reference results. These comparisons demonstrate that the performance of our present direct simulation is acceptable, and the obtained data can be used for decomposition analysis.
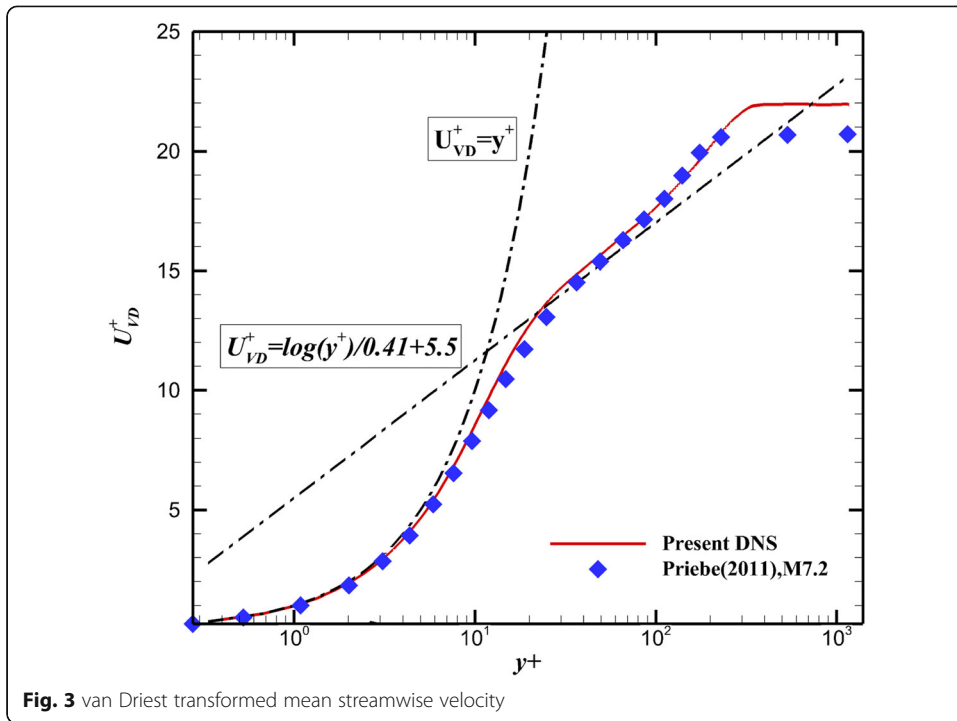

Fig. 2 The instantaneous magnitude of the vortical structures
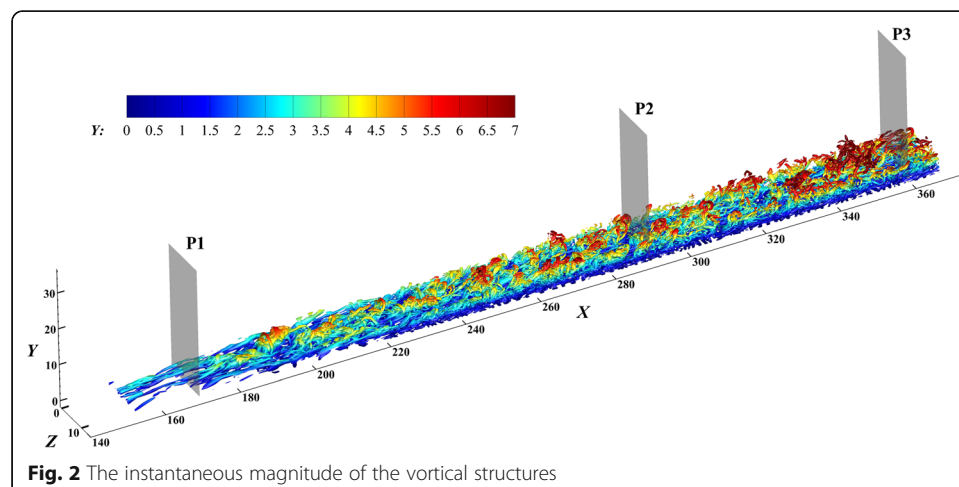
Fig. 3 van Driest transformed mean streamwise velocity
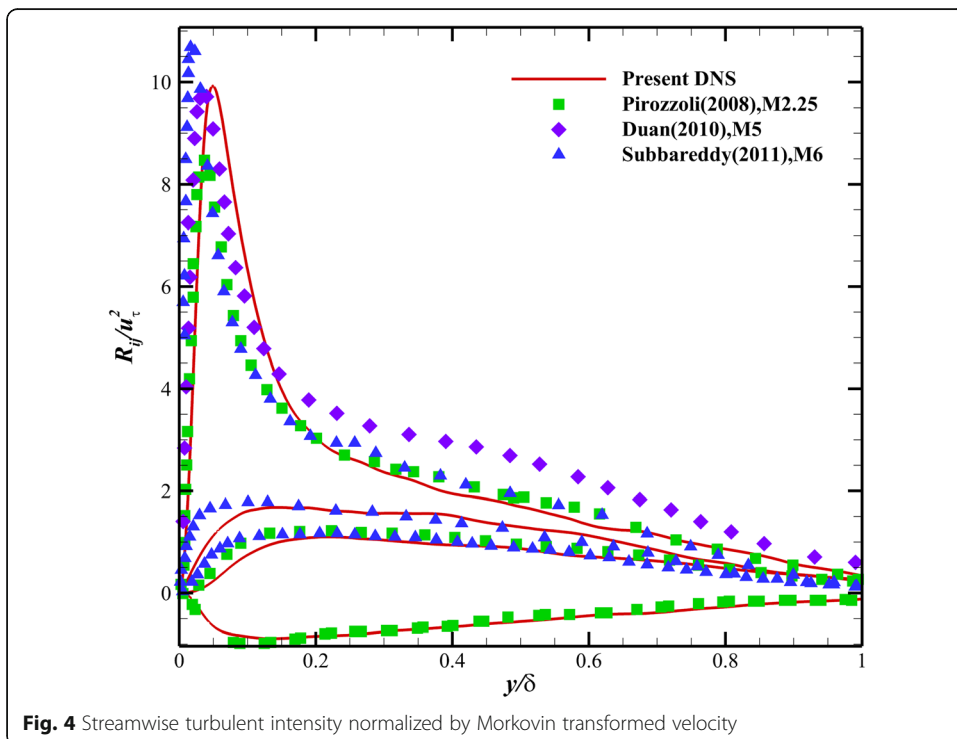

Fig. 4 Streamwise turbulent intensity normalized by Morkovin transformed velocity

Table 2 Setup of the reference simulations

	Ma	(L_x, L_y, L_z)	(N_x, N_y, N_z)	$(\Delta x^+, \Delta y^+, \Delta z^+)$
Priebe (2011)	7.2	$(27.0\delta_{ref}, 14.2\delta_{ref}, 10.0\delta_{ref})$	(840, 150, 768)	(7.5, 0.3, 3.0)
Pirozzoli (2008)	2.0	$(25.0\delta_{ref}, 3\delta_{ref}, 3.7\delta_{ref})$	(1809, 180, 225)	(4.5, 0.95, 4.5)
Duan (2010)	5.0	$(7.5\delta_{ref}, 16.7\delta_{ref}, 1.9\delta_{ref})$	(384, 110, 256)	(7.7, 0.33, 2.9)
Subbareddy (2011)	6.0	NA	(5400, 175, 175)	(30.0, 0.5, 25.0)
Present DNS	6.0	$(64.0\delta_{ref}, 5.4\delta_{ref}, 2.2\delta_{ref})$	(1151, 320, 149)	(7.9, 0.36, 3.4)

4.2 Contributions of different energy transport processes

The contributions of different energy transport processes to the wall heat flux at different streamwise locations, e.g. P1-P3 are calculated according to Eq. (10). The ratios of the contributions of the terms in Eq. (10) to the reconstructed heat flux coefficient $C_{h,decom}$ and the relative errors are presented in Table 3. The relative error is defined as $Error = (C_{h,decom} - C_{h,0})/C_{h,0} \times 100\%$, where $C_{h,0}$ is the time-averaged heat flux coefficient. The relative errors are very small in both transitional and turbulent regions. In Table 3, it is found that the work done by the molecular stresses ($C_{h,5}$) and Reynolds stresses ($C_{h,6}$) plays dominant roles in heat production. The sum of the contributions of these two terms takes over 2.7 times of $C_{h,0}$ in the transition region and 1.9 times in the turbulent region. The contributions of the heat conduction ($C_{h,1}$) and the turbulent transport of heat ($C_{h,2}$) are negative, which indicates both processes act as the transporters of the heat and carry the extra heat to the outer regions of the boundary layer. The magnitude of $C_{h,1}$ and $C_{h,5}$ gets greater in the turbulent region due to the large gradient of the profiles. On the other hand, $C_{h,2}$ and $C_{h,6}$ in the transitional region are much greater than those in the turbulent region, because of the quick nonlinear development of the structures.

The trends of the contributions can be further assessed when more sample locations are considered. The trends of the contributions in the transition process are presented in Fig. 5. In addition, the instantaneous density gradient and the time-averaged heat flux coefficient are also presented to show the overall evolution procedure. The symbols in the line of $C_{h,i}$ indicate different sample locations (from left to right labelled as X0 to X10). The first sample point (X0) is located in the laminar region; therefore, the work of the molecular stress and the heat conduction is the main factor affecting the wall heat. After entering the transition region, the effects of the Reynold stresses become dominant. Moreover, a rapid variation of $C_{h,6}$ is observed in the transition region due to the nonlinear development of the coherent structures. While in the turbulent region, an equilibrium state is reached and a smooth variation is obtained. The trends of contributions of the heat conduction $C_{h,1}$ and the molecular stresses $C_{h,5}$ are very smooth in both transition and turbulent regions, which indicate they are not sensitive to the change of the turbulent fluctuations. In addition, the effects of the molecular

Table 3 Contributions of the terms in Eq. (10)

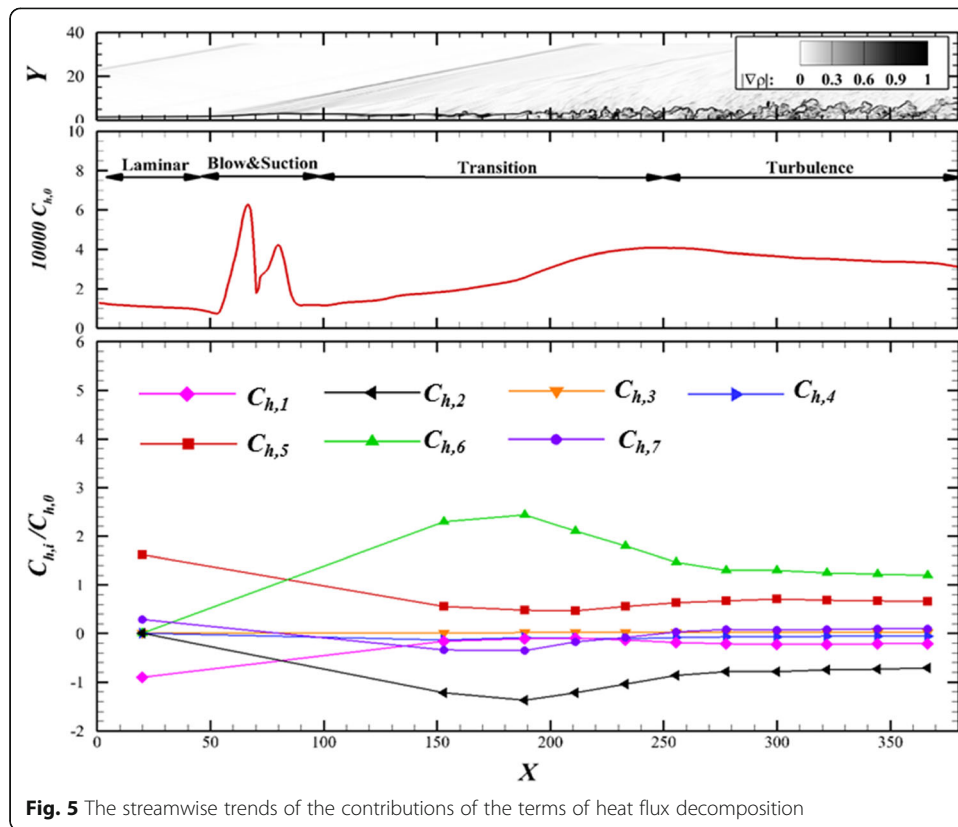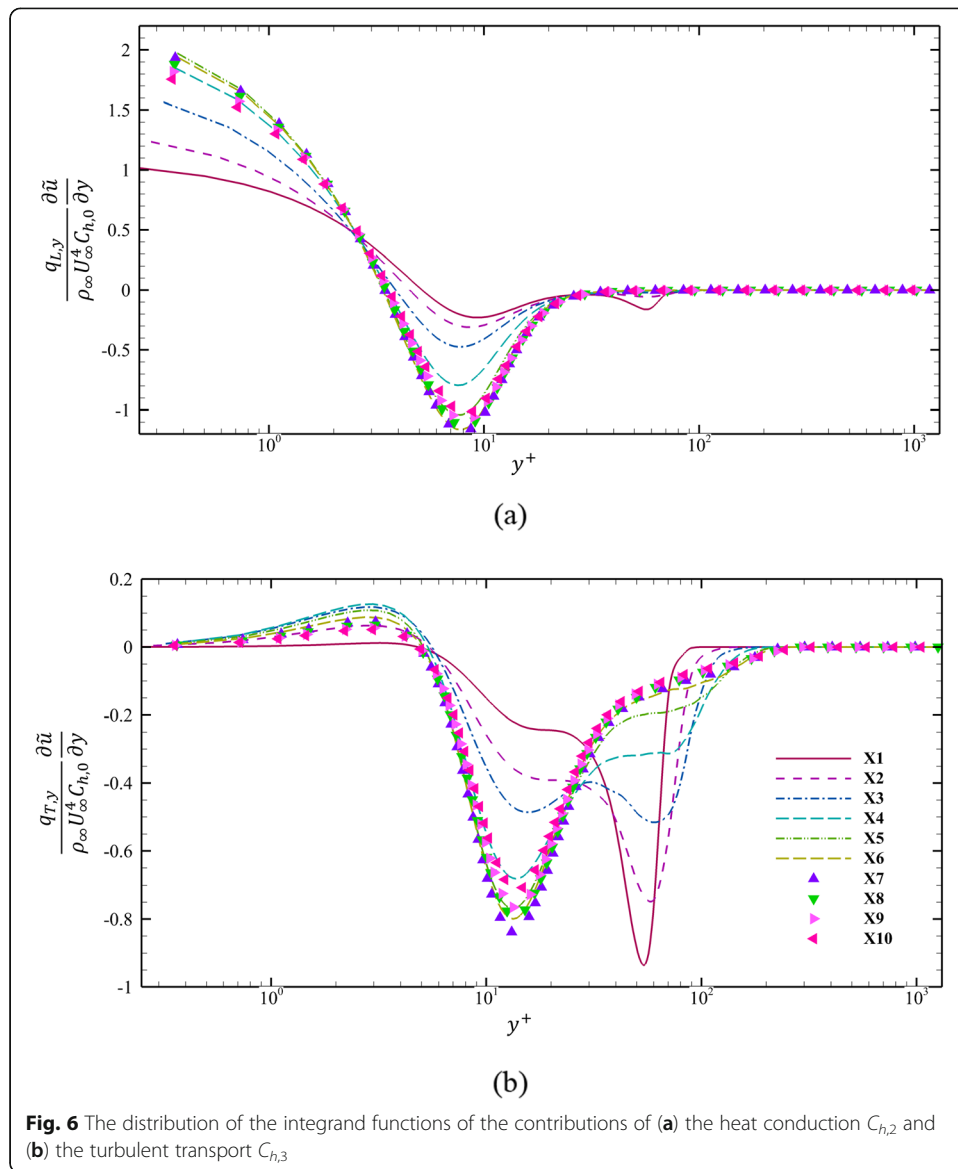|	$C_{h,1}/C_{h,decom}$	$C_{h,2}/C_{h,decom}$	$C_{h,3}/C_{h,decom}$	$C_{h,4}/C_{h,decom}$	$C_{h,5}/C_{h,decom}$	$C_{h,6}/C_{h,decom}$	$C_{h,7}/C_{h,decom}$	$C_{h,0}$	$C_{h,decom}$	Err
P1	−0.111	−1.379	0.018	−0.084	0.478	2.437	−0.359	1.195E-4	1.183E-4	1.00%
P2	−0.213	−0.785	0.012	−0.072	0.673	1.299	0.086	1.825E-4	1.819E-4	0.33%
P3	−0.208	− 0.713	0.015	− 0.054	0.662	1.200	0.098	1.616E-4	1.620E-4	0.25%

Fig. 5 The streamwise trends of the contributions of the terms of heat flux decomposition

diffusion ($C_{h,3}$), the turbulent transport of TKE ($C_{h,4}$) and the streamwise heterogeneity ($C_{h,7}$) are very small during the whole transition.

4.3 Key normal locations affecting the wall heat

The key normal locations where the structures affect the wall heat can be attained by analyzing the integrand functions of the terms in Eq. (10). Two main transporters, i.e., the heat conduction ($C_{h,2}$) and the turbulent transport ($C_{h,3}$) and two main contributors, i.e., the work by molecular stresses ($C_{h,5}$) and Reynolds stresses ($C_{h,6}$) are analyzed in this section.

The integrand functions of the heat conduction ($C_{h,2}$) and the turbulent transport ($C_{h,3}$) are presented in Fig. 6. The lines in the figure denote the locations in the transitional region and the symbols are the locations in the turbulent region. The contribution of $C_{h,2}$ is positive when the normal locations are near the wall due to the positive temperature gradient. When y^+ reaches 10, a valley is observed, which is formed by the decrease of the temperature after the peak of the mean temperature. Compared with the integrand function of $C_{h,2}$, two valleys are observed in the integrand functions of $C_{h,3}$. The first valley is located at $y^+ \approx 65$, the magnitude of the valley reduces and finally disappears as the locations move downstream. The second valley is located at around $y^+ = 10$, which corresponds to the buffer layer of the turbulent boundary layer. The valley will get larger as the locations move downstream.

Fig. 6 The distribution of the integrand functions of the contributions of (**a**) the heat conduction $C_{h,2}$ and (**b**) the turbulent transport $C_{h,3}$

The key normal locations of the work by molecular stresses ($C_{h,5}$) and Reynolds stresses ($C_{h,6}$) are analyzed in Fig. 7. The positive contribution of $C_{h,5}$ is mainly located in the regions near the wall. As the normal location increases, the integrand function will decrease and a valley is formed around y^+ = 10. Meanwhile, a peak is observed around y^+ = 10 in the integrand function of contribution of $C_{h,6}$. The peak is located in the buffer layer of the boundary layer. In addition, in the transition process, the magnitude of the peak will get larger as the streamwise distance increases.

5 Conclusions

In this paper, we proposed a new decomposition formula for the wall heat flux. And the performance of the formula has been well demonstrated by DNS results of a hypersonic transitional boundary layer.

Fig. 7 The distribution of the integrand of the contribution of work done by (**a**) molecular stresses $C_{h,5}$ and (**b**) Reynolds stresses $C_{h,6}$
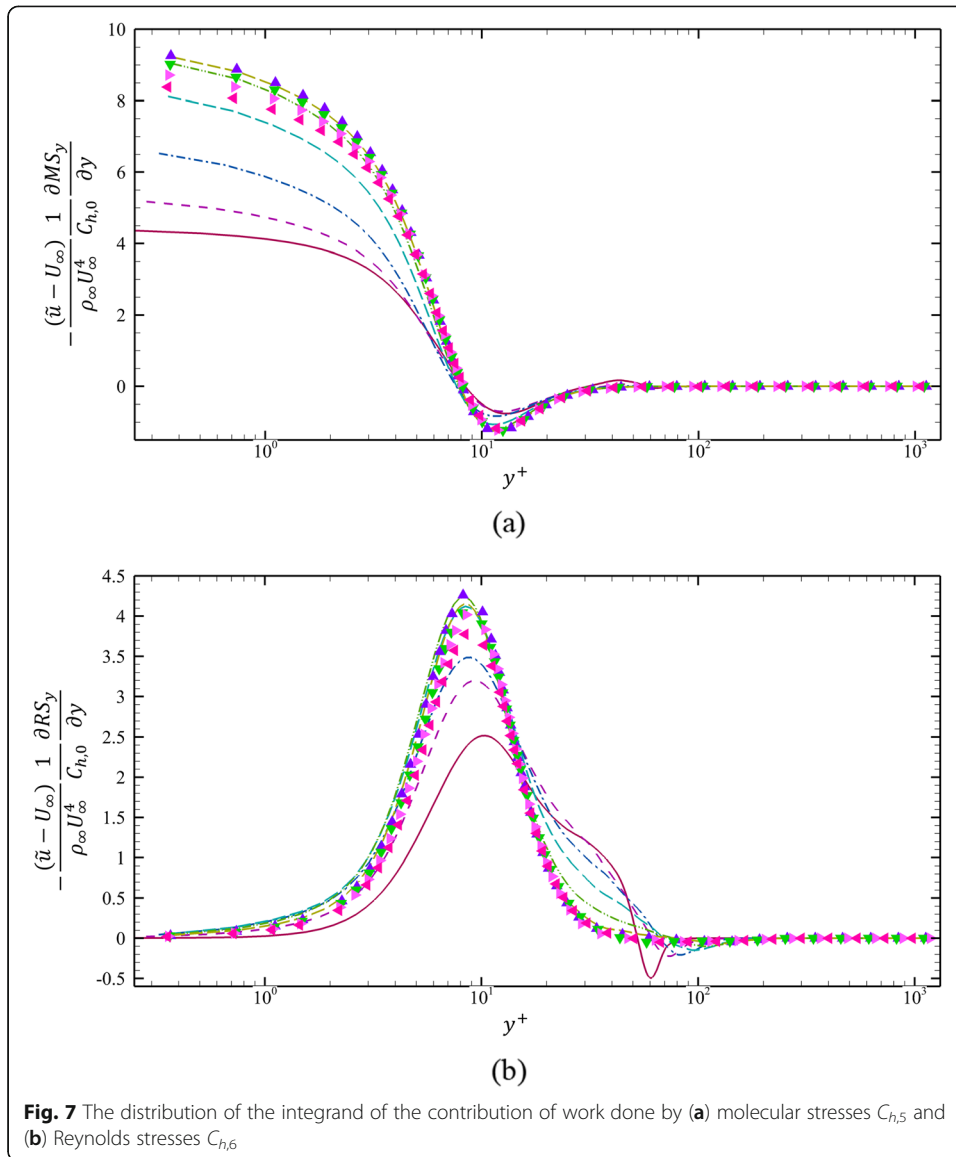
(1) Through this formula, the wall heat flux can be decomposed into contributions of seven terms, i.e., the heat conduction, turbulent transport of heat, molecular diffusion, turbulent transport of TKE, molecular stresses, the Reynolds stresses and the streamwise heterogeneity.

(2) The contributions of each term can be calculated quantitatively. For the present case, it is found that the heat flux produced by the work done by Reynolds stresses and molecular stresses is much higher than the time-averaged heat flux on the wall. The heat conduction and turbulent convection will carry the extra heat into the outer part of the boundary layer.

(3) The structures in the buffer layer ($y^+ = 10$) play a dominant role in the production and transfer of the heat flux for the present simulation. Moreover, the contributions of the heat conduction and the molecular stresses are mainly affected by the gradient of the temperature.

(4) As the assumption used in the derivation is only the spanwise homogeneity and nonslip wall, this formula can be applied in the analysis of the heat transfer of a hypersonic transitional/turbulent boundary layer at high Mach numbers, which can be employed to identify the main factors affecting the wall heating and provide good guidance for the design of the thermal protection system.

Declarations

Author details
[1]State Key Laboratory of Aerodynamics, Mianyang 621000, Sichuan, China. [2]Computational Aerodynamics Institute, China Aerodynamics Research and Development Center, Mianyang 621000, Sichuan, China.

References
1. Tiliakos N, DeSorbo J, Martin N, Viti V, Laurence S, Rabin O (2020) A roadmap for obtaining and implementing heat flux measurements in the hypersonic environment. AIAA Paper 2020-2448. https://doi.org/10.2514/6.2020-2448
2. Roy CJ, Blottner FG (2006) Review and assessment of turbulence models for hypersonic flows. Prog Aerosp Sci 42(7-8): 469–530. https://doi.org/10.1016/j.paerosci.2006.12.002
3. Hopkins EJ, Inouye M (1971) An evaluation of theories for predicting turbulent skin friction and heat transfer on flat plates at supersonic and hypersonic Mach numbers. AIAA J 9(6):993–1003. https://doi.org/10.2514/3.6323
4. Huang PG, Coleman GN, Bradshaw P (1995) Compressible turbulent channel flows: DNS results and modelling. J Fluid Mech 305:185–218. https://doi.org/10.1017/S0022112095004599
5. Chen T, Liu T, Wang L, Chen S (2019) Relations between skin friction and other surface quantities in viscous flows. Phys Fluids 31(10):107101. https://doi.org/10.1063/1.5120454
6. Abe H, Antonia RA (2017) Relationship between the heat transfer law and the scalar dissipation function in a turbulent channel flow. J Fluid Mech 830:300–325. https://doi.org/10.1017/jfm.2017.564
7. Kim S, Kim M, Kim K (2002) A direct integration approach for the estimation of time-dependent boundary heat flux. KSME Int J 16(10):1320–1326. https://doi.org/10.1007/BF02983839
8. Ebadi A, Mehdi F, White CM (2015) An exact integral method to evaluate wall heat flux in spatially developing two-dimensional wall-bounded flows. Int J Heat Mass Transf 84:856–861. https://doi.org/10.1016/j.ijheatmasstransfer.2014.12.068
9. Fukagata K, Iwamoto K, Kasagi N (2005) Novel turbulence control strategy for simultaneously achieving friction drag reduction and heat transfer augmentation. Proc 4th Int Symp Turbulence and Shear Flow Phenomena. Williamsburg, Virginia, pp 307–312
10. Liu J, Zhao P, Lei M, Yang S, Nemati H (2020) Numerical investigation of spatial-developing turbulent heat transfer in forced convections at different supercritical pressures. Int J Heat Mass Transf 159:120128. https://doi.org/10.1016/j.ijheatmasstransfer.2020.120128
11. Ghosh S, Foysi H, Friedrich R (2010) Compressible turbulent channel and pipe flow: similarities and differences. J Fluid Mech 648:155–181. https://doi.org/10.1017/S0022112009993004
12. Zhang P, Xia Z (2020) Contribution of viscous stress work to wall heat flux in compressible turbulent channel flows. Phys Rev E 102(4):043107. https://doi.org/10.1103/PhysRevE.102.043107
13. Fukagata K, Iwamoto K, Kasagi N (2002) Contribution of Reynolds stress distribution to the skin friction in wall-bounded flows. Phys Fluids 14(11):L73–L76. https://doi.org/10.1063/1.1516779
14. Renard N, Deck S (2016) A theoretical decomposition of mean skin friction generation into physical phenomena across the boundary layer. J Fluid Mech 790:339–367. https://doi.org/10.1017/jfm.2016.12
15. Sun D, Guo Q, Li C, Liu P (2020) Assessment of optimized symmetric fourth-order weighted essentially non-oscillatory scheme in direct numerical simulation of compressible turbulence. Comput Fluids 197:104383. https://doi.org/10.1016/j.compfluid.2019.104383

16. Li C, Guo Q, Sun D, Zhang H (2020) Aerothermal prediction of hypersonic flow around spherical capsule model using IDDES approach. Int J Modern Physics B 34(14-16):2040078. https://doi.org/10.1142/S0217979220400780
17. Sun D, Chen J, Li C, Liu P, Guo Q, Yuan X (2020) On the wake structure of a micro-ramp vortex generator in hypersonic flow. Phys Fluids 32(12):126111. https://doi.org/10.1063/5.0030975
18. Sun D, Guo Q, Li C, Liu P (2019) Direct numerical simulation of effects of a micro-ramp on a hypersonic shock wave/boundary layer interaction. Phys Fluids 31(12):126101. https://doi.org/10.1063/1.5123453
19. Guo Q, Sun D, Li C, Liu P, Zhang H (2020) A new discontinuity indicator for hybrid WENO schemes. J Sci Comput 83:28. https://doi.org/10.1007/s10915-020-01217-w
20. Jiang G, Shu C (1996) Efficient implementation of weighted ENO schemes. J Comput Phys 126(1):202–228. https://doi.org/10.1006/jcph.1996.0130
21. Pirozzoli S, Grasso F, Gatski TB (2004) Direct numerical simulation and analysis of a spatially evolving supersonic turbulent boundary layer at M=2.25. Phys Fluids 16(3):530–545. https://doi.org/10.1063/1.1637604
22. Wilcox DC (2006) Turbulence modeling for CFD, 3rd edn. DCW Industries Inc, La Canada
23. Li W, Fan Y, Modesti D, Cheng C (2019) Decomposition of the mean skin-friction drag in compressible turbulent channel flows. J Fluid Mech 875:101–123. https://doi.org/10.1017/jfm.2019.499
24. Hunt J, Wray A, Moin P (1988) Eddies, streams, and convergence zones in turbulent flows. Proceedings of the Summer Program 1988 of the Center for Turbulence Research, N89-24555, pp 193-208
25. Priebe S, Martín MP (2011) Direct numerical simulation of a hypersonic turbulent boundary layer on a large domain. AIAA Paper 2011-3432
26. Duan L, Beekman I, Martín P (2010) Direct numerical simulation of hypersonic turbulent boundary layers. Part 2. Effect of wall temperature. J Fluid Mech 655:419–445. https://doi.org/10.1017/S0022112010000959
27. Pirozzoli S, Bernardini M, Grasso F (2008) Characterization of coherent vortical structures in a supersonic turbulent boundary layer. J Fluid Mech 613:205–231. https://doi.org/10.1017/S0022112008003005
28. Subbareddy PK, Candler GV (2011) DNS of transition to turbulence in a hypersonic boundary layer. AIAA Paper 2011–3564. https://doi.org/10.2514/6.2011-3564

Publisher's Note